RESEARCH ARTICLE

Distinct Patterns of Clonal Evolution Drive Myelodysplastic Syndrome Progression to Secondary Acute Myeloid Leukemia

Tiffany Guess[1,2], Chad R. Potts[1], Pawan Bhat[3], Justin A. Cartailler[1], Austin Brooks[1], Clinton Holt[4], Ashwini Yenamandra[2], Ferrin C. Wheeler[2], Michael R. Savona[1,3,5], Jean-Philippe Cartailler[6], and P. Brent Ferrell Jr[1,3,5]

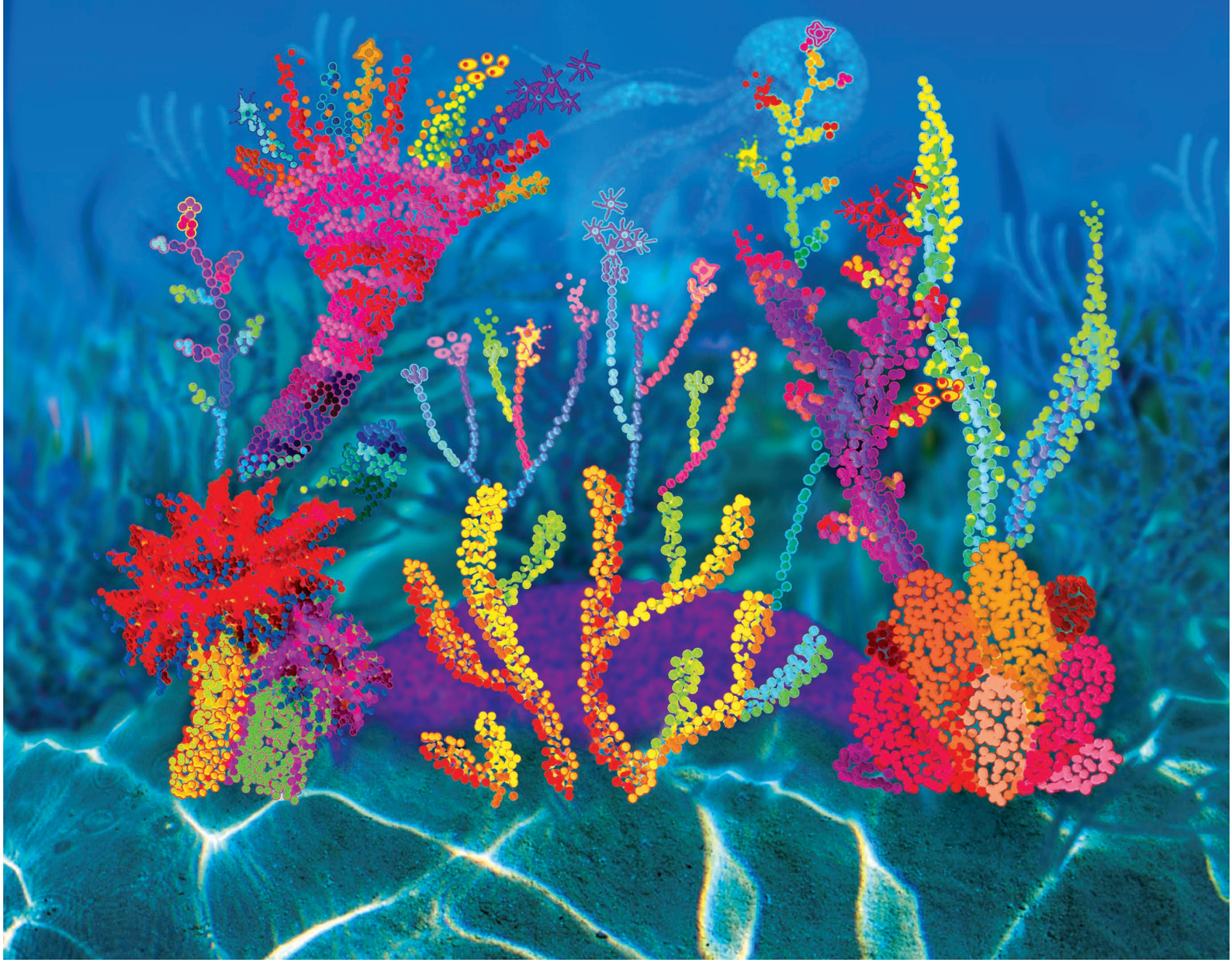

ABSTRACT Clonal evolution in myelodysplastic syndrome (MDS) can result in clinical progression and secondary acute myeloid leukemia (sAML). To dissect changes in clonal architecture associated with this progression, we performed single-cell genotyping of paired MDS and sAML samples from 18 patients. Analysis of single-cell genotypes revealed patient-specific clonal evolution and enabled the assessment of single-cell mutational cooccurrence. We discovered that changes in clonal architecture proceed via distinct patterns, classified as static or dynamic, with dynamic clonal architectures having a more proliferative phenotype by blast count fold change. Proteogenomic analysis of a subset of patients confirmed that pathogenic mutations were primarily confined to primitive and mature myeloid cells, though we also identify rare but present mutations in lymphocyte subsets. Single-cell transcriptomic analysis of paired sample sets further identified gene sets and signaling pathways involved in two cases of progression. Together, these data define serial changes in the MDS clonal landscape with clinical and therapeutic implications.

SIGNIFICANCE: Precise clonal trajectories in MDS progression are made possible by single-cell genomic sequencing. Here we use this technology to uncover the patterns of clonal architecture and clonal evolution that drive the transformation to secondary AML. We further define the phenotypic and transcriptional changes of disease progression at the single-cell level.

See related article by Menssen et al., p. 330 (31).

See related commentary by Romine and van Galen, p. 270.

INTRODUCTION

For patients with myelodysplastic syndromes (MDS), the transformation to secondary acute myeloid leukemia (sAML) brings poor therapeutic response and a significantly shortened lifespan (1–3). Mutated hematopoietic cells exist within a complex ecosystem, where both intrinsic and extrinsic forces influence the process of clonal evolution (4, 5). This clonal evolution is fundamental to disease progression and therapeutic resistance in MDS and sAML (6–11). Foundational studies using bulk next-generation sequencing have leveraged mutational frequencies and statistical modeling to impute the clonal identity and extract patterns of clonal evolution (10, 12, 13). Whole-genome sequencing data first demonstrated that approximately 85% of bone marrow cells in seven MDS patients were clonal and that at least one new pathogenic mutation accompanied progression to sAML (8). In each of the cases reported, clonal evolution occurred through the linear acquisition and expansion of new mutant subclones. A subsequent study investigated 11 patients with samples at MDS and sAML by whole-exome sequencing combined with a larger cohort of 44 MDS-to-sAML samples analyzed via targeted sequencing (12). This analysis demonstrated that clonal evolution could occur through either the linear evolution of subclones or branching evolution, with clonal competition from parallel subclones (12). A recent review summarized these and other published studies comparing the genetics of paired MDS and sAML samples and confirmed that linear and branching patterns occur (14). Furthermore, they revealed that signaling and transcription factor mutations are more abundant at sAML, whereas almost all mutations present in MDS samples persist in sAML. Ultimately, however, bulk DNA sequencing (DNA-seq) is not able to directly confirm cell-specific mutational identities.

Novel approaches using single-cell DNA-seq (scDNA-seq) have enabled precise clonal assignments (13). This technology provides a key advantage by defining mutational presence within single cells of mutationally diverse samples. Single-cell sequencing has already provided insights regarding the heterogeneity of the MDS stem cell pool and the presence of clonal competition within this pool (13). High-throughput scDNA-seq has also recently been leveraged by a number of researchers to investigate clonal evolution in clonal hematopoiesis, as well as myeloid and lymphoid malignancies (15–22). Results from these studies have revealed mutational associations, genotype/phenotype relationships, and the increasing clonal complexity of myeloid malignancies throughout the course of therapy (15, 16, 22). Furthermore, a recent study analyzing a large cohort of AML data has found that clonal heterogeneity, mutational frequency, evolution pattern, and mutational order correlate with clinical outcomes (23). Thus, understanding clonal architecture and change over time could lead to translational impact in myeloid malignancies.

Given these advances in single-cell genotyping and potential clinical impact, we hypothesized that scDNA-seq would better characterize clonal shifts upon MDS progression. Here,

[1]Department of Medicine, Division of Hematology/Oncology, Vanderbilt University Medical Center (VUMC), Nashville, Tennessee. [2]Department of Pathology, Microbiology, and Immunology, VUMC, Nashville, Tennessee. [3]Program in Cancer Biology, Vanderbilt University School of Medicine, Nashville, Tennessee. [4]Program in Chemical and Physical Biology, Vanderbilt University School of Medicine, Nashville, Tennessee. [5]Vanderbilt-Ingram Cancer Center, Nashville, Tennessee. [6]Creative Data Solutions Shared Resource, Center for Stem Cell Biology, Vanderbilt University, Nashville, Tennessee.

Corresponding Author: P. Brent Ferrell Jr, Vanderbilt University Medical Center, 777 Preston Research Building, 2220 Pierce Avenue, Nashville, TN 37232. Phone: 615-875-8619; E-mail: brent.ferrell@vumc.org

Blood Cancer Discov 2022;3:316–29

doi: 10.1158/2643-3230.BCD-21-0128

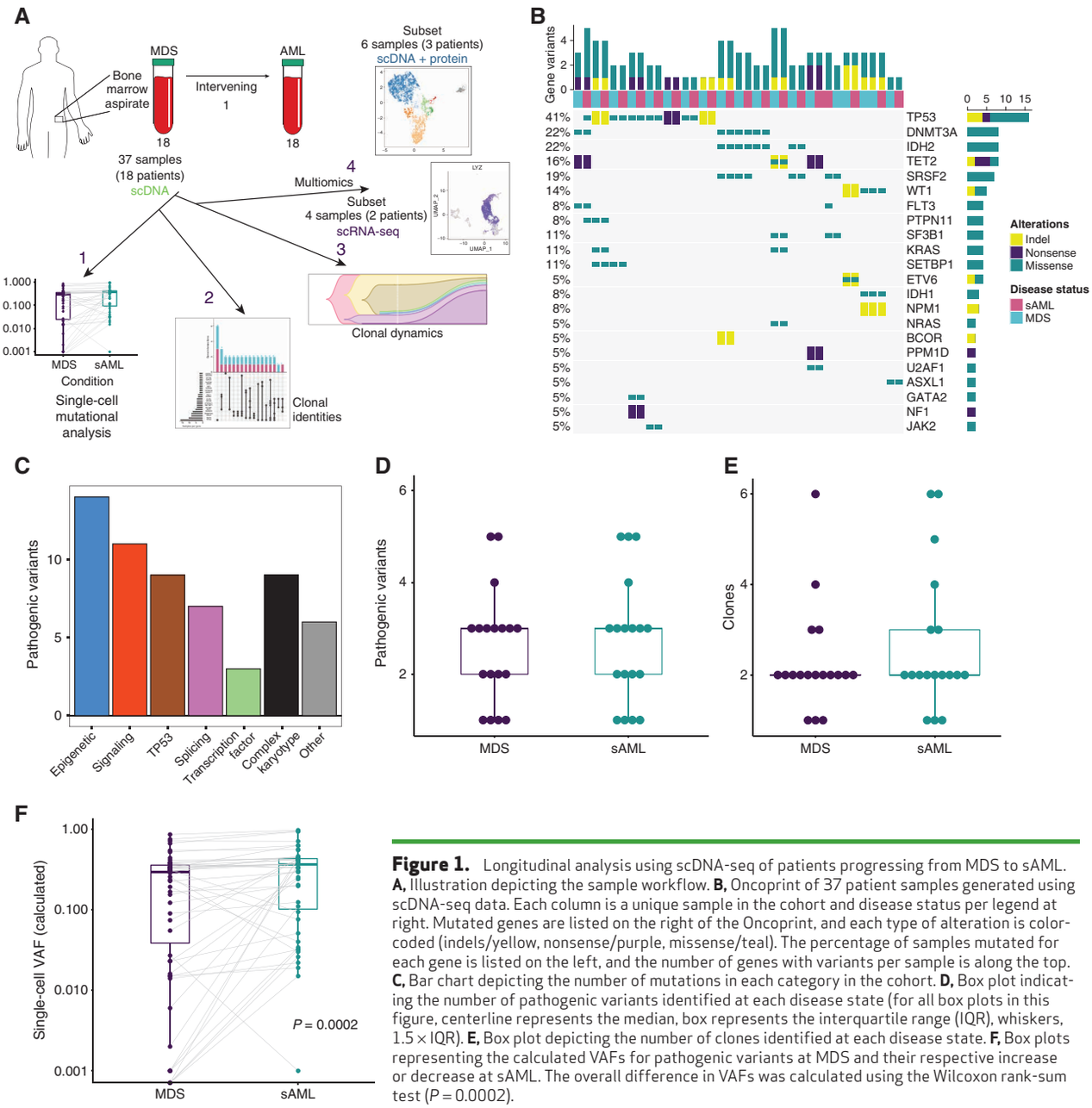

Figure 1. Longitudinal analysis using scDNA-seq of patients progressing from MDS to sAML. **A,** Illustration depicting the sample workflow. **B,** Oncoprint of 37 patient samples generated using scDNA-seq data. Each column is a unique sample in the cohort and disease status per legend at right. Mutated genes are listed on the right of the Oncoprint, and each type of alteration is color-coded (indels/yellow, nonsense/purple, missense/teal). The percentage of samples mutated for each gene is listed on the left, and the number of genes with variants per sample is along the top. **C,** Bar chart depicting the number of mutations in each category in the cohort. **D,** Box plot indicating the number of pathogenic variants identified at each disease state (for all box plots in this figure, centerline represents the median, box represents the interquartile range (IQR), whiskers, 1.5 × IQR). **E,** Box plot depicting the number of clones identified at each disease state. **F,** Box plots representing the calculated VAFs for pathogenic variants at MDS and their respective increase or decrease at sAML. The overall difference in VAFs was calculated using the Wilcoxon rank-sum test ($P = 0.0002$).

we use single-cell genomics to analyze clonal, phenotypic, and transcriptional changes in paired samples of MDS and sAML.

RESULTS

Single-Cell DNA Sequencing of Paired Samples Resolves Mutational Characteristics of MDS and sAML

Using an scDNA-seq amplicon panel composed of 45 commonly mutated genes, we analyzed 37 paired longitudinal bone marrow samples from 18 patients (Fig. 1A; Supplementary Fig. S1A). The mutational landscape for all samples is depicted in Fig. 1B, whereas patient characteristics for the cohort are shown in Supplementary Table S1. A total of 136,710 individual cells were genotyped, averaging 3,695 cells per sample (range, 209–9,792 cells/sample) and 169,352 reads per cell (range, 12,016–1,834,736; Supplementary Fig. S1B and S1C; Supplementary Table S2). Single-cell variant allele frequencies (VAF) were overall well correlated with results from bulk-sequencing ($R = 0.75$, $P \leq 0.0001$, Pearson correlation; Supplementary Fig. S1D). Variants in *ASXL1* were genotyped at a low frequency by scDNA-seq, which others have observed (18). The calculated median allele dropout (ADO) rate was between 1.9% and 15.8% per sample, with a median of 6.80% overall, consistent with previously published ADO rates for this platform (Supplementary Table S3; refs. 17, 24, 25). We identified 50 pathogenic or likely pathogenic recurrent mutations (44 unique mutations) within 50 clones (Fig. 1B and C; Supplementary Fig. S1C; Supplementary Table S4). As

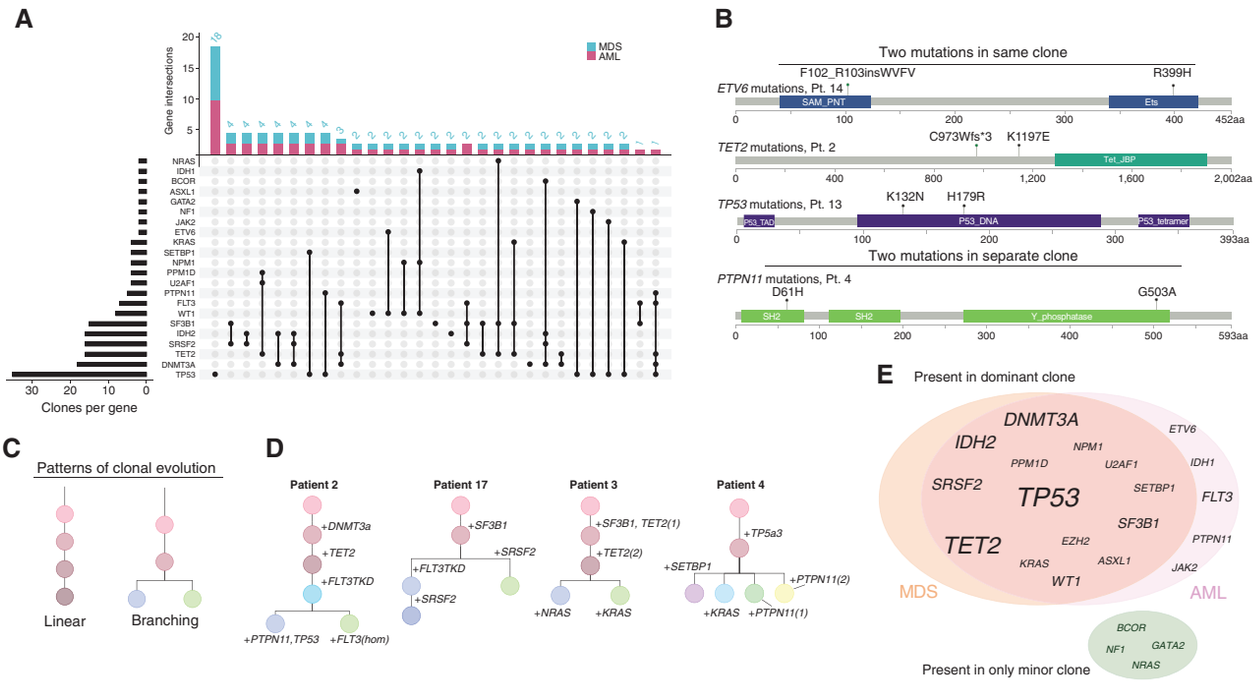

Figure 2. Single-cell mutational identities define clonal evolution. **A,** UpSet plot depicting comutational occurrences in MDS and sAML clones. The number of times a gene was involved in a clone is listed on the left side of the plot for the entire cohort. The number of times each gene combination was detected in a clone is listed at the top of the plot. **B,** Illustration of multiple mutations within the same gene. This phenomenon was observed in four patients, three instances occurring within the same clone and one occurring in different clones. Specific gene residues are listed in each instance. **C,** Patterns of clonal evolution depicted as phylogenies. **D,** Phylogenies for samples with a branching evolution and signaling mutations. **E,** Venn diagram of variants in the dominant clone. Mutations in the genes listed in the green circle occurred only in minor clones at either MDS or sAML. Font size is representative of the number of times mutations were observed in each gene.

expected, the number of mutations correlated with the number of clones per sample (Supplementary Fig. S1E). We further characterized gene functional categories in our cohort. We found mutations in genes from six functional categories, similar to previously published categories, but with some minor differences in gene composition from these studies (Supplementary Table S5; refs. 26–29). Using functional categories for mutations in myeloid malignancy, 14 of the mutations were epigenetic (which included mutations in *DNMT3a, IDH1/2, TET2, ASXL1*, and *BCOR*), 11 were signaling (which included *FLT3, JAK2, NF1, NRAS, KRAS*, and *PTPN11*), 9 were in *TP53*, 7 were splicing (which included *U2AF1, SRSF2*, and *SF3B1*), 3 were in transcription factors (which included *GATA2* and *ETV6*), and 6 mutations in genes outside of these categories (which included *SETBP1, WT1*, and *NPM1*; Fig. 1C; refs. 14, 26). The number of mutations and clones did not differ between MDS and sAML (Fig. 1D and E). *TP53* (18%, 9/50 mutations) and *DNMT3A* (8%, 4/50) were the most frequently mutated genes in the cohort. All *DNMT3A* variants were the R882H missense variant, whereas variants in *TP53* differed in each instance. Missense mutations accounted for most variants detected by single-cell sequencing (37 total, 31 unique; Fig. 1B). The mean scVAF for identified pathogenic mutations at MDS increased at sAML (24.2% vs. 33.1%, $P = 0.0002$ by the paired Wilcoxon rank-sum test; Fig. 1F). Within the patient cohort, all but one patient was treated with a DNA methyltransferase inhibitor (DNMTi; 17/18), either decitabine or azacitidine for MDS, but therapy differed thereafter and at sAML (Supplementary Table S1).

Single-Cell Mutational Identity Defines MDS Clonal Architecture

scDNA-seq clarified the cooccurrence of pathogenic variants within individual cells. The two most common intraclonal mutational cooccurrences were *IDH2/DNMT3A* (three individuals) and *IDH2/SRSF2* (three individuals; Fig. 2A; Supplementary Fig. S2A). Other mutational cooccurrences were notable, including both cases of subclonal *SETBP1* mutations (patients 4 and 12) coexisting with *TP53* mutations. Four patients had two pathogenic mutations in the same gene. Of these, three cooccurred in the same subclone (*ETV6, TET2*, and *TP53*), and one was found in two separate subclones (*PTPN11*; Fig. 2B). Such subclonal competition was common in cases with RAS pathway mutations (classified as *PTPN11*, *KRAS*, *NRAS*, and *NF1*). Two cases of MDS/sAML harbored at least two distinct subclones with different RAS pathway mutations (patients 3 and 4; Fig. 2C). Competing parallel subclones with RAS pathway mutations were also observed in an independent cohort in six additional RAS family mutants, as well as in previous scDNA investigations of AML (15, 30, 31). The presence of signaling mutations was enriched in samples with branching clonal evolution in our cohort (6/6 cases branching cases with signaling mutations, 0/12 without, Fisher exact test, $P = 1e{-}5$; Fig. 2C and D). We further

Table 1. Cooccurrence of RAS pathway mutations in MDS

Gene A	Gene B	Neither	A not B	B not A	Both	Log_2 Odds ratio	*P* value	*q* value	Tendency
NRAS	*KRAS*	3,600	447	139	45	1.383	<0.001	<0.001	Cooccurrence
NRAS	*PTPN11*	3,566	448	173	44	1.018	<0.001	<0.001	Cooccurrence
KRAS	*PTPN11*	3,846	168	201	16	0.866	0.025	0.038	Cooccurrence
NRAS	*NF1*	3,062	442	94	3	–2.177	0.001	0.003	Mutual exclusivity

referenced publicly available genomic data from a data set of MDS samples representing 4,231 samples/patients using the cBioPortal to analyze RAS pathway mutation cooccurrence (19, 32, 33). Here, we confirmed statistically significant cooccurrences of two RAS pathway mutational pairs, including *NRAS* and *KRAS* ($q < 0.001$), *NRAS* and *PTPN11* ($q < 0.001$), and *KRAS* and *PTPN11* ($q < 0.038$). *NRAS* and *NF1* were mutually exclusive ($q = 0.003$; data set was queried on *KRAS*, *NRAS*, *PTPN11*, and *NF1* mutations; Table 1).

Overall, the mutational number and heterogeneity did not differ between MDS and sAML. The mean number of mutations per clone was similar between disease states (2.15 and 2.25, respectively; two-tailed Student *t* test, $P = 0.62$; Supplementary Fig. S2B), as was the Shannon diversity index of subclones (Supplementary Fig. S2C). We further analyzed mutations in dominant, or most abundant, clones in each case. *DNMT3A* and *TET2* mutations were present in the founding, or earliest detectable clone if founding clone was not identified, except for two cases in which a *TET2* mutation occurred following a previous *DNMT3A* or *TET2* mutation (patients 2 and 3; Supplementary Fig. S3A–S3C). When present, *DNMT3A* and TET2 mutations were always found in the dominant clone in sAML (5/5 cases). *TP53* variants appeared in both the dominant and founding clones in 87.5% (7/8) of cases with at least one *TP53* mutation. Similarly, variants in *TP53* were the most common to occur as the sole variant in a clone, with 18 *TP53*-only clones detected in the cohort (Fig. 2A). Variants in the genes *PTPN11, IDH1*, and *FLT3* occurred in the dominant clone only upon progression to sAML, though they were found in a small number of cells in the corresponding MDS samples (Fig. 2E; Supplementary Fig. S4).

Progression of MDS Occurs via Distinct Patterns of Clonal Evolution and Architecture Change

To test the hypothesis that changes in the mutational landscape accompany disease progression, we analyzed the clonal phylogenies and changes from MDS to sAML in each patient. In this analysis, we distinguished between the pattern of clonal evolution, which can be inferred from scDNA-seq data from one sample and articulates the sample's phylogenetic history, and the pattern of clonal architecture change, which is defined by comparison of clonal frequencies between at least two samples (Figs. 2C and 3A). For each case, we analyzed both patterns of clonal evolution and clonal architecture change. We found that most patients (67%, 12/18) displayed linear clonal evolution (defined based on scDNA data), in which only one subclone arises from any previous clone or subclone. The remaining six cases demonstrated branching clonal evolution (Supplementary Fig. S3). With respect to clonal architecture change, we identified three distinct patterns: static and dynamic, which were further classified based on the type of clonal change (SNV or chromosomal; Fig. 3A). Six of 18 patients (33.3%) exhibited a Static clonal architecture, which displayed minimal clonal change (<10% change for any minor clone) and without the emergence of a new dominant clone (e.g., patient 3; Fig. 3B). The second pattern consisted of an emergent dominant clone in sAML (5/18, 27.8%), indicative of a subclonal sweep coinciding with progression (e.g., patient 2; Fig. 3B; ref. 5). Here, we define an emergent dominant subclone as a clone that was small or undetectable in the MDS sample. Given that these variants were detected by scDNA-seq, we call this pattern Dynamic SNV (Dynamic-S). In all Static and all but two Dynamic-S cases, karyotypes were normal or had fewer than three abnormalities (Supplementary Table S1). The third group (38.9%, 7/18) displayed minimal changes in single-cell variant-defined clonal architecture, like the Static group; however, this group was characterized by karyotypes which increased in complexity at sAML, representing a dynamic-chromosomal landscape (e.g., patient 11; Fig. 3B). Thus, we termed this group Dynamic-Chromosomal (Dynamic-C). Though performed on a small number of single cells, clinical karyotypes can identify the subclonal architecture of large genetic changes. Dynamic-C cases demonstrated clonal evolution marked by increasing loss or gain of chromosomal material, including new deletions of partial and whole chromosomes, duplications, and translocations. Rather than small driver mutations (detected via amplicon sequencing) defining the clonal structure, as in the Dynamic-S group, transformation in this pattern coincided with a deteriorating chromosomal landscape, with numerous gains or losses of chromosomal material (karyotype shown for patient 11; Fig. 3C and D; list of changes for all Dynamic-C patients in Supplementary Table S6).

We further investigated the existence of these patterns in MDS progression using data from an independent cohort (31). Among 12 cases that were analyzed with whole-genome sequencing for which a clonal analysis was done, we identified one case of static evolution (UPN 280498), whereas the remaining 11 represented a dynamic change in clonal architecture (6 Dynamic-S and 5 Dynamic-C cases; ref. 31).

Clinical Correlates of Clonal Evolution

There was a significantly higher blast fold change (log_2 scale) in the combined Dynamic group (Supplementary Fig. S4A). Blast fold change did not correlate with time to progression, and time between samples was similar among the groups (Supplementary Fig. S4B). A comparison of blast fold change within each group demonstrated a significantly greater blast increase in Dynamic-S compared with Static cases (Supplementary Fig. S4C and S4D). The Dynamic-C

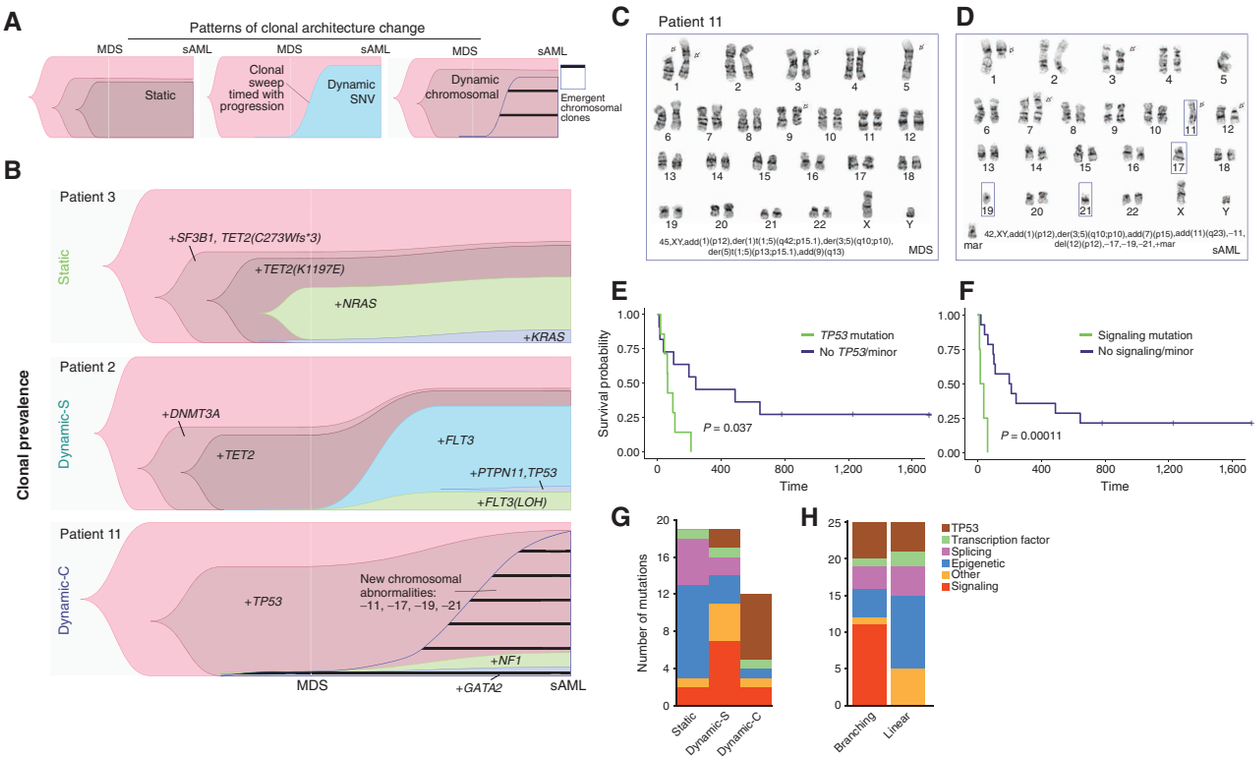

Figure 3. scDNA-seq characterizes clonal trajectories during disease progression. **A,** Representative TimeScape plots of the three types of clonal progression observed in the cohort. **B,** Clonal prevalence over time of three patients, each with a distinct pattern of clonal progression from MDS to sAML: Static, Dynamic SNV, and Dynamic Chromosomal, respectively. The leftmost clone in each plot is the parent clone from which all cells were derived (no mutations detected). Karyotypes at (**C**) MDS and (**D**) sAML for patient 11 demonstrating dynamic-chromosomal clonal progression. **E,** Kaplan–Meier curve of sAML survival when the signaling mutation was present in the dominant clone. **F,** Kaplan–Meier curve for TP53 samples when present in the dominant clone (for both Kaplan–Meier curve, log-rank test *P* value is shown). **G** and **H,** Mutation type distribution per clonal architecture and clonal evolution pattern.

group had significantly fewer pathogenic mutations and clones (by scDNA-seq) compared with patients with Static or Dynamic-S clonal evolution (Supplementary Fig. S4E and S4F). The cohort had three patients with treatment-related MDS, 2 of 7 patients in the Dynamic-C group and one patient in the Dynamic-S group. There was no statistically significant difference in survival after sAML among the groups, though median survival for all patients was dismal at only 106 days (Supplementary Fig. S4G). Though survival did not vary based on the clonal architecture change, we hypothesized that the mutational identity of the sAML-dominant clone could correlate with the outcome. In a univariate analysis, the presence of a signaling mutation or the presence of a *TP53* mutation in the dominant sAML subclone was found to correlate with sAML survival (Fig. 3E and F). To understand the multivariate effect of these mutations, we calculated a Cox proportional hazards model for death based on age over 60, sex, *TP53* status, and IPSS-R. In this model, signaling (HR = 559; 95% CI, 15.6–2 × 10^4) and *TP53* (HR = 15.7; 95% CI, 2–118) mutations in the dominant sAML subclone were both associated with increased risk of death ($P = 0.0005$ and $P = 0.007$, respectively; Supplementary Table S7; Supplementary Fig. S5A–S5E; residuals of model). An IPSS-R group of intermediate (I) was associated with decreased risk of death in the model (HR 0.003; 95% CI, 0.00003–0.25 and HR 0.03; 95% CI, 0.003–0.47, respectively; Supplementary Table S7).

Characteristic Genomic Changes Accompany Dynamic Clonal Architecture

We next characterized the genomic alterations of each architectural change or clonal evolution pattern (Fig. 3G and H; Supplementary Fig. S3). The Dynamic-C group was enriched for *TP53* mutations (6/7 within the group vs. 2/11 in other groups, Fisher exact test, $P = 0.009$; Fig. 3G). As the disease progressed, the allele burden of *TP53* mutations or deletions increased in all cases (Supplementary Table S6; Supplementary Fig. S3C). Increased *TP53* allelic state at the sample level has recently been associated with worse outcomes in MDS; thus, it is not surprising that single-cell TP53 allelic state would increase at progression (34, 35). By contrast, signaling mutations often accompanied Dynamic-S architectural change (36). Here, we observed an enrichment of signaling mutations in the dominant, or largest, subclone of Dynamic-S sAML samples compared with all other samples (3/5 vs. 0/13, Fisher exact test, $P = 0.01$; Fig. 3G), which included two *FLT3* tyrosine kinase domain (TKD) mutations (patients 2 and 17) and a *PTPN11* mutation (patient 4; Supplementary Fig. S3B). We also observed a similar enrichment of signaling mutations in cases with branching clonal evolution (Fig. 3H).

Within some cases, the variant that ultimately defined the dominant subclone at disease progression was often detected

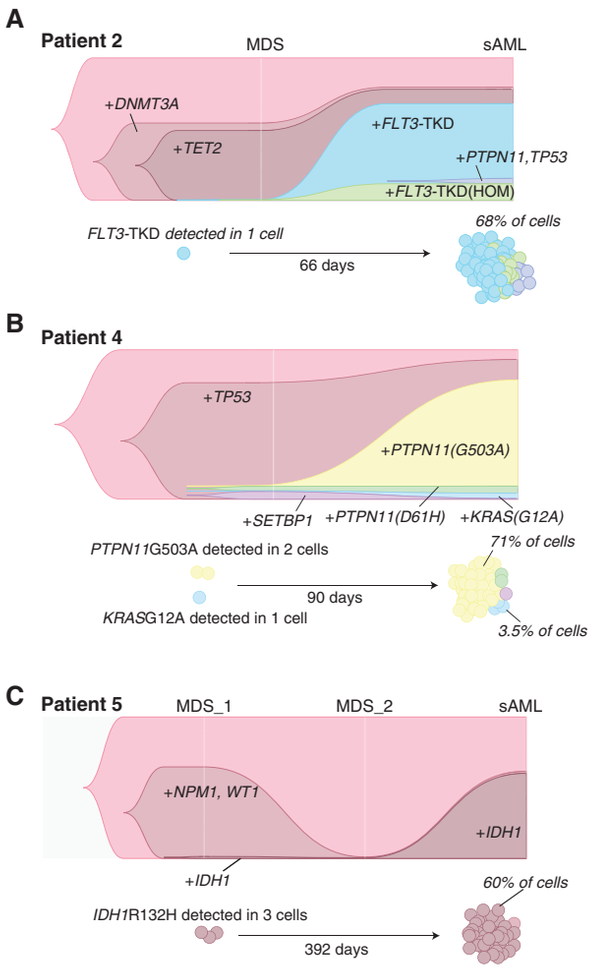

Figure 4. Subclonal expansion of rare cells in dynamic architectural change. **A,** Patient 2 clonal prevalence and depiction of the expansion of rare clones with *FLT3*-TKDmut from MDS to sAML. **B,** Patient 4 rare cell expansion of the *PTPN11mut* subclone. **C,** Patient 5, rare cell expansion of the *IDH1mut* subclone.

at MDS in fewer than 10 cells. However, the presence of these exact mutations in larger numbers at a second, or third, time point, allowed us to confirm these rare cells as subclones in the MDS sample. In patient 2, the MDS-to-sAML transition was characterized by the acquisition of an *FLT3* mutation to the *DNMT3A* + *TET2* clone that dominated the MDS mutational landscape (Fig. 4A). The growth of the *FLT3* clone in this patient progressed rapidly, with the diagnosis of sAML made just two months later. One cell in the MDS sample was found to have an *FLT3* mutation, yet this mutation was present in 68% of cells sequenced at sAML (Fig. 4A). In patient 4, the *PTPN11*G503A clone and the *KRAS*G12A clone were found in two cells and one cell, respectively, at MDS, but these mutations were in 71% and 3.5% of total cells sequenced at sAML (Fig. 4B). Analysis of three samples (two MDS and one sAML) from patient 5 found only three cells at the first MDS timepoint with an *IDH1*R132H mutation. All mutations were undetectable at a second, posttreatment, time point, and then the *IDH1* clone became the dominant clone (60% of cells) in driving recurrent disease in sAML (Fig. 4C). Despite its ability to capture some mutations in a small number of cells, scDNA-seq did not detect an *FLT3*-internal tandem duplication (ITD) for one patient in the Dynamic-S group (patient 17), which was present on bulk-sequencing at a VAF of 0.31 in the MDS sample. Interestingly, this patient was treated with sorafenib with azacitidine after this MDS sample was collected and subsequently gained an *FLT3*-TKD mutation, while losing the *FLT3*-ITD in sAML, a known resistance mechanism to sorafenib and other FLT3 inhibitors (37).

Clonal Mutations Are Enriched in Primitive and Mature Myeloid Cells and Rare in Lymphoid Cells

To dissect genotype/phenotype relationships, we used scDNA-seq combined with antibody–oligonucleotide conjugates (AOC) for key cell-surface markers on hematopoietic cells (Supplementary Table S8; refs. 15, 16, 38). Three MDS/sAML sample pairs (six samples) were stained, sequenced, and analyzed. Two of these sample sets were from the Dynamic-S cohort (patients 14 and 17), whereas the third was from the Static cohort (patient 18). To visualize cellular organization based on immunophenotype, we embedded AOC data in a two-dimensional map using uniform manifold approximation and projection (UMAP) combined with hierarchical density-based clustering (HDBSCAN) to visualize the data (39). Each cluster was assigned a cell type name based on the expert assessment of immunophenotype, though given the limited panel size, assignment of cell identity overlapped across clusters. For patient 17, the visualization of single-cell genotypes on the surface-marker–based UMAP revealed a strong bias of all three mutations for myeloid cells, though rare T cells and NK cells did harbor mutations (Fig. 5A and B). Single-cell visualization of surface-marker abundance identified primitive and mature myeloid cells as well as lymphocyte populations (Fig. 5C). In patient 18, primitive cells show a large expansion at sAML, including hematopoietic stem and progenitor-like cell clusters, from MDS to sAML (Fig. 5D–F). Similarly, the visualization of genotypes within individual cells revealed rare mutant T and NK cells harboring mutant genotypes (Fig. 5E and F). Analysis of mutated versus nonmutated cells for founding mutations in patients 17 and 18 (*SF3B1* K666N and *IDH2* R172K, respectively) in all cell clusters demonstrated rare mutations in all lymphoid cell subsets identified as well as MDS to sAML increase in more primitive cell types (Fig. 5G and H). Analysis of patient 14 data revealed a similar enrichment of mutations in the primitive ($CD117^+$ cell cluster) and rare mutations in T cells (Supplementary Fig. S6A–S6F).

Single-Cell RNA Sequencing Identifies Transcriptional Changes Associated with MDS Progression

We performed single-cell RNA sequencing (scRNA-seq) on both MDS and sAML samples of patients 3 and 17 to examine transcriptional changes that define MDS therapy resistance and progression. These cases both feature dominant clone signaling mutations, but different clonal architecture changes (dynamic vs. static). Analysis of paired samples allowed each patient's MDS sample to serve as a baseline

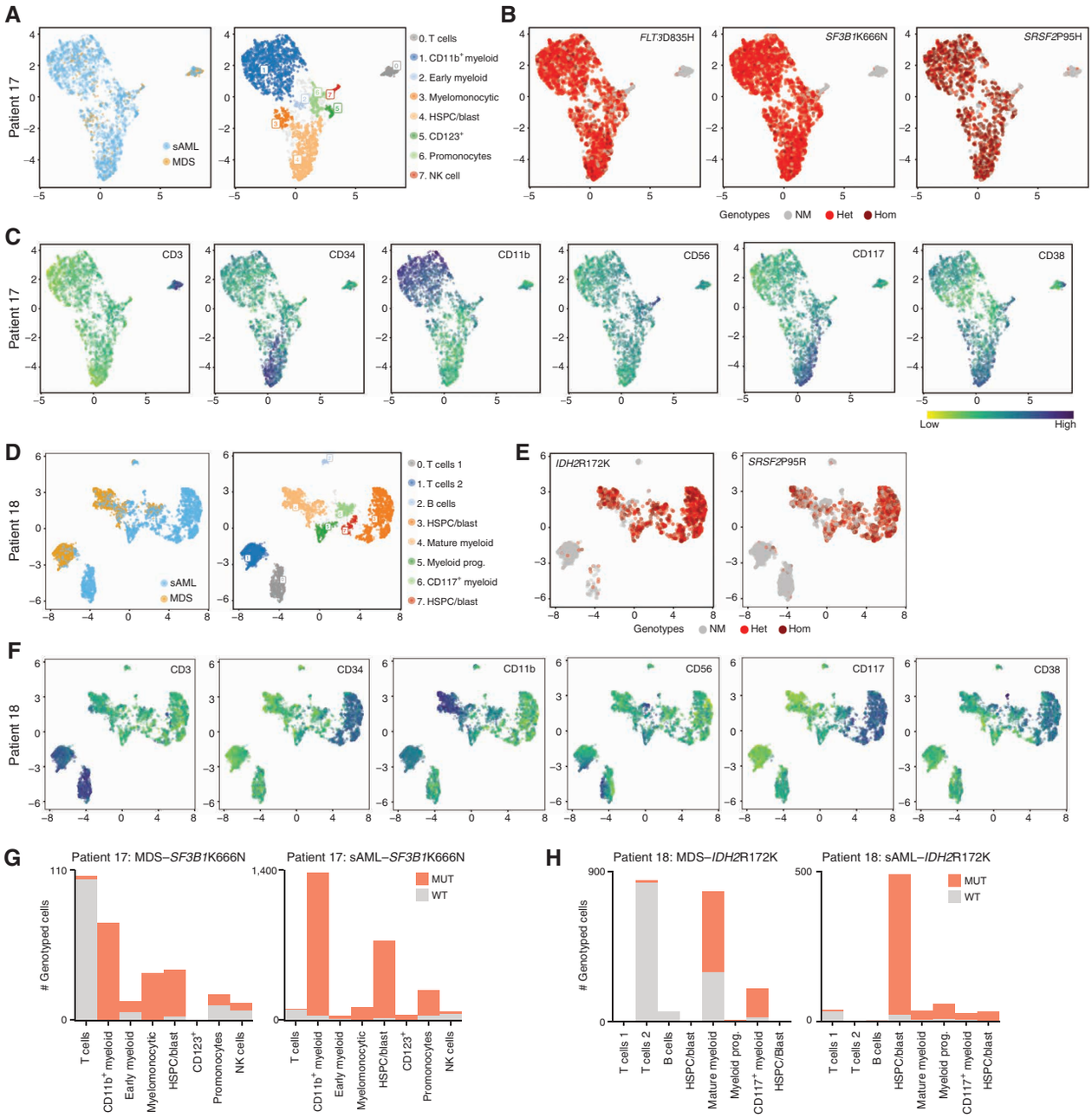

Figure 5. Combined protein and DNA analysis reveals mutational identities of both myeloid and lymphoid lineages. **A,** UMAP embeddings (patient 17) mapped on cell-surface marker levels colored by samples or by HDBSCAN clusters. Clusters were identified by immunophenotype and named for cell type by immunophenotype. **B,** Genotypes are shown for each mapped cell (only cells for which each genotype was known). Code for each variant is no mutation (NM), heterozygous (Het), or homozygous (Hom). **C,** Surface-marker expression of major markers used to define cell type. **D–F,** Similar to **A**–**C**, but with patient 18. **G** and **H,** Cell cluster–based analysis of the proportion of mutated cells MDS to sAML for *SF3B1* (patient 17) or *IDH2* (patient 18).

to dissect transcriptional changes in the sAML sample. We visualized samples from each patient's scRNA-seq data with UMAP, followed by clustering and expert naming of cell subsets (Fig. 6A and B; refs. 39, 40).

In patient 17, we confirmed the presence of both early and more mature myeloid leukemia cells seen in the sample with the clinical pathology data, which identified approximately 45% blast and blast equivalents in the sAML (which included myeloblasts, monoblasts, and promonocyte-like cells in this acute myelomonocytic leukemia). Clinical flow cytometry identified similar numbers of primitive myeloblasts [15% of whole bone marrow (WBM) cells, positive for CD34] and more promonocyte-like blast equivalents (19% of WBM, negative for CD34), confirming the heterogeneity seen with both of our single-cell modalities (Fig. 6A). Overall, clusters within the primitive clusters increased from MDS to sAML, whereas

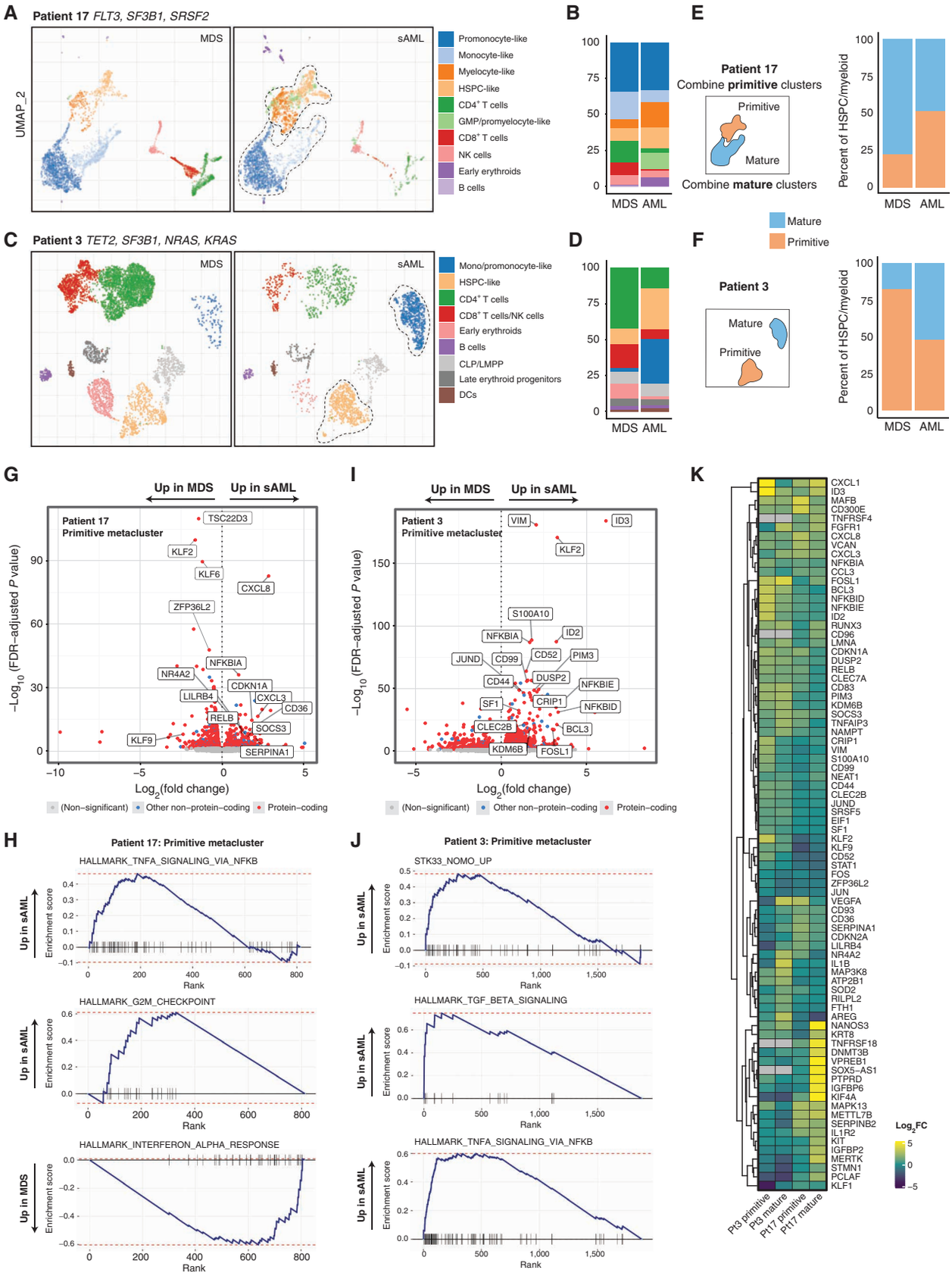
A
Patient 17 FLT3, SF3B1, SRSF2
MDS
sAML
UMAP_2
Promonocyte-like
Monocyte-like
Myelocyte-like
HSPC-like
CD4+ T cells
GMP/promyelocyte-like
CD8+ T cells
NK cells
Early erythroids
B cells
B
MDS AML
E
Patient 17
Combine primitive clusters
Primitive
Mature
Combine mature clusters
Percent of HSPC/myeloid
C
Patient 3 TET2, SF3B1, NRAS, KRAS
Mono/promonocyte-like
HSPC-like
CD4+ T cells
CD8+ T cells/NK cells
Early erythroids
B cells
CLP/LMPP
Late erythroid progenitors
DCs
D
F
Patient 3
G
Up in MDS
Up in sAML
Patient 17
Primitive metacluster
−Log10 (FDR−adjusted P value)
Log2(fold change)
TSC22D3
KLF2
KLF6
CXCL8
ZFP36L2
NFKBIA
NR4A2
CDKN1A
LILRB4
CXCL3
CD36
RELB
SOCS3
KLF9
SERPINA1
(Non−significant)
Other non−protein−coding
Protein−coding
I
Patient 3
Primitive metacluster
VIM
ID3
KLF2
S100A10
NFKBIA
ID2
JUND
CD99
CD52
PIM3
CD44
DUSP2
NFKBIE
SF1
CRIP1
NFKBID
CLEC2B
BCL3
KDM6B
FOSL1
K
CXCL1
ID3
MAFB
CD300E
TNFRSF4
FGFR1
CXCL8
VCAN
CXCL3
NFKBIA
CCL3
FOSL1
BCL3
NFKBID
NFKBIE
ID2
RUNX3
CD96
LMNA
CDKN1A
DUSP2
RELB
CLEC7A
CD83
PIM3
KDM6B
SOCS3
TNFAIP3
NAMPT
CRIP1
VIM
S100A10
CD99
NEAT1
CD44
CLEC2B
JUND
SRSF5
EIF1
SF1
KLF2
KLF9
CD52
STAT1
FOS
ZFP36L2
JUN
VEGFA
CD93
CD36
SERPINA1
CDKN2A
LILRB4
NR4A2
IL1B
MAP3K8
ATP2B1
SOD2
RILPL2
FTH1
AREG
NANOS3
KRT8
TNFRSF18
DNMT3B
VPREB1
SOX5−AS1
PTPRD
IGFBP6
KIF4A
MAPK13
METTL7B
SERPINB2
IL1R2
KIT
IGFBP2
MERTK
STMN1
PCLAF
KLF1
Log2FC
Pt3 primitive
Pt3 mature
Pt17 primitive
Pt17 mature
H
Patient 17: Primitive metacluster
HALLMARK_TNFA_SIGNALING_VIA_NFKB
HALLMARK_G2M_CHECKPOINT
HALLMARK_INTERFERON_ALPHA_RESPONSE
Up in sAML
Up in MDS
Enrichment score
Rank
J
Patient 3: Primitive metacluster
STK33_NOMO_UP
HALLMARK_TGF_BETA_SIGNALING
HALLMARK_TNFA_SIGNALING_VIA_NFKB

the mature cells decreased slightly (Fig. 6B). To facilitate a comparison of transcriptional profiles based on disease time point and cell type, we computationally merged the primitive (HSPC-, GMP/promyelocyte-, and myelocyte-like) and mature (promonocyte- and monocyte-like) myeloid clusters into two metaclusters, primitive and mature (Fig. 6C). We performed a similar analysis with patient 3, which had a static architecture with stable dominant *KRAS* and minor *NRAS* subclones, which differed from patient 17 in that both early and mature metaclusters were made up of only one subcluster and both population had large increases at sAML relative to other cell types (Fig. 6D–F). We next performed differential expression (DE) and single-cell gene set enrichment analysis (scGSEA) on pseudo-bulk transcriptional data from the primitive and mature metaclusters from MDS or sAML for each patient (Fig. 6G–K; Supplementary Fig. S7A–S7D). The expanding primitive metacluster from patient 17 demonstrated an increase in signaling molecules, including *CXCL8* (IL8), *CXCL3*, *RELB*, and *NR4A2*. Additionally, there were increases in suppressors of signaling pathways, *NFKBIA*, *SOCS3*, and the surface receptor *LILRB4*, which has been implicated in leukemia immune escape (Fig. 6G; ref. 41). Downregulated in this primitive cluster were genes involved in the differentiation of myeloid cells, including *KLF2* and *KLF6* (42). Top gene sets for primitive cells from patient 17 sAML included those related to cell-cycle progression and TNFα signaling via NF-κB, whereas interferon-α and interferon-γ signaling were enriched in the MDS sample (Fig. 6H). Within the primitive cell cluster for patient 3, some of the top transcripts with increased expression in sAML included signaling genes (*JUND, FOSL1*), intermediate filament gene vimentin (*VIM*), and surface-marker genes associated with leukemia stem cells (*CD52, CD99*, and *CD44*; Fig. 6I; refs. 43–46). Interestingly, patient 3 demonstrated enrichment in gene sets for TGFβ and TNFα signaling in sAML, as well as those related to intermediate filament signaling (serine/threonine kinase STK33) in *KRAS*-mutant leukemia cells (Fig. 6J; ref. 47). Top genes in the mature metacluster for patient 17 included downregulation of several major histocompatibility complex genes (e.g., *CD74, HLA-DQA1*, and *HLA-DPA1*) with an increase in inflammatory cytokines (*CXCL8*, *CXCL2*), whereas gene set enrichment included proliferation-associated cell cycle (G2M_CHECKPOINT) and DNA replication gene sets (E2F_TARGETS), whereas interferon gene sets were enriched in MDS (Fig. 6K; Supplementary Fig. S7A and S7B). The mature metacluster for patient 3 showed an increase in inflammatory genes at sAML, including *IL1B*, and enrichment of interferon gene sets in the sAML sample, along with inflammatory and KRAS-associated signaling gene sets (Supplementary Fig. S7C and S7D). These data outline a framework for a personalized analysis of transcriptional enrichment to discover potentially critical pathways for disease progression.

DISCUSSION

Progression of MDS to sAML is a clinically devastating event. Since the first fundamental studies demonstrated the clonal origins of this transformation, the field has focused on defining clonal populations with ever-increasing granularity (10, 12, 13). Recent studies using scDNA-seq have focused primarily on AML, demonstrating clonal architectures that become progressively more complex as myeloid neoplasia advances (15, 16). Here we dissect patterns of change in clonal architecture and clonal evolution upon progression to sAML. Our data document differing complexity in MDS clonal transformation. Whereas some patients have relatively stable patterns of clonal complexity, others show striking changes. The former, which we refer to as the Static group, displays minimal changes in architecture while still transforming to sAML, suggesting that genomic evolution might not explain disease progression entirely. Given that all of the samples in the Static group had founder mutations in DNA methylation genes (*DNMT3A/TET2/IDH1/2*), it is possible that changes in the epigenome drive cell proliferation and accelerate blast growth through progressively disrupted differentiation (48–50). In contrast, the Dynamic groups possessed large clonal architectural changes, with respect to either chromosomally-defined (Dynamic-C group) or smaller variant-defined (Dynamic-S group) clonal changes. With the Dynamic-S cases, the emergent mutations tended to be those classically associated with sAML and enriched for signaling effector mutations (12, 14). These signaling effectors present potential therapeutic strategies for this group. By contrast, the Dynamic-C group was enriched for *TP53* mutations and characterized by karyotypes of increasing complexity during disease progression. These changes do not present clear therapeutic targets given the lack of specific mutations beyond *TP53*. Although our analysis identified that clonal architecture changes do not correlate with survival, these genomic associations, namely, signaling or *TP53* mutations within the dominant clone at sAML, did associate with poor survival at sAML. Though our multivariate model revealed significant effects, any survival effects are limited here and would need to be confirmed in a larger cohort. Ultimately, this study is limited by a small cohort size, heterogeneous treatment, and the possibility that an amplicon panel would miss some driver mutations, due to either technical limitations or simply not having a gene represented on the panel. With respect to subclonal structure, we demonstrated that RAS family mutations often occur in multiple competing subclones, demonstrating convergent evolution. This also raises the question about whether these subclones enable the emergence or selection of similar clones.

We also examined the relationships between genotype and phenotype in our cohort. In a subset of our cases, we show that mutations are ubiquitous in primitive and mature

Figure 6. scRNA-seq of longitudinal samples identify transcriptional gene sets that accompany disease progression. **A,** Gene expression-derived UMAP embedding of all cells from scRNA-seq of two samples from patient 17, clustered with HDBSCAN and then labeled by cell type according to transcriptional signature. The dotted line encapsulates primitive and mature cells (for **E**, **F**). **B,** Number of cells per cluster shown and change from MDS to sAML. **C** and **D,** UMAP and cluster distribution for patient 3 as in **A**–**B**. **E** and **F,** Cells mapped from each time point and patient separately with a depiction of the creation of metaclusters that are either labeled primitive or mature. **G,** Differentially expressed genes for primitive metacluster for patient 17, with selected top significant genes labeled. **H,** GSEA plots for patient 17 primitive metacluster. **I,** Differentially expressed genes for patient 3 primitive metacluster. **J,** Patient 3 GSEA plots for primitive metacluster. **K,** Heatmap depicting differentially expressed genes across all metaclusters with heat based on $\log_2$ fold change increase.

myeloid cells at sAML. We further show that lymphocytes may possess mutations observed in myeloid cells, even those mutations that are more prominent in sAML. The mutational involvement of lymphocytes indicates contribution by mutant stem cell clones still capable of multilineage output in clonal hematopoiesis. Although this has been observed by others in myeloid malignancies and aplastic anemia, the implications for immune function have not been fully elucidated (9, 51–53). Confirming frequency and understanding whether these mutated lymphocytes have some pathogenic or disease-promoting effects are areas for future interest. Further, our scRNA-seq analysis revealed gene expression associated with disease progression. We identified downregulation of HLA genes, upregulation of intermediate filaments, upregulation of LILRB4, and inflammatory signaling as potential mechanisms of transformation, which have been previously associated with AML (41, 54, 55). Future analysis of larger scRNA-seq data sets of sAML may further identify disease targets.

Despite the fact that approximately one third of patients diagnosed with MDS will progress to sAML, there are few therapies that alter this risk, and only a transplant offers a chance at a cure (56). Deepening our understanding of this disease progression by combining mutational identity, cellular phenotypes, and transcriptional signatures holds tremendous promise to realize new therapeutic avenues, the hope to identify preemptive measures that can prevent leukemic transformation before it occurs.

METHODS

Reagents

Tapestri-related reagents, including AOCs, were purchased from Mission Bio, Inc. Dextran sulfate was purchased from Research Products International. Custom oligonucleotides for i5/i7 indexing and 5′ Biotin were purchased from Integrated DNA Technologies (IDT). Human TruStain FcX and Ampure XP beads were purchased from BioLegend and Beckman Coulter, respectively. Streptavidin beads and Dulbecco's PBS were purchased from Thermo Fisher. Single-cell RNA reagents were purchased from 10× Genomics. Custom myeloid bulk DNA sequencing kits were purchased from Archer Dx.

Patient Samples

Patients included were diagnosed with MDS and progressed to sAML between 2015 and 2019. Pathologic diagnosis of both MDS and sAML was assigned according to the World Health Organization criteria (57). Patients were enrolled via written informed consent for sample collection, and bone marrow aspirates were collected at both stages of disease and processed by the Hematologic Tissue Repository at Vanderbilt University Medical Center (VUMC). Bone marrow mononuclear cells were cryopreserved and stored in liquid nitrogen until use. All patient tissue and data were obtained with written informed consent and used according to the protocol approved by the local Institutional Review Board and conducted in accordance with the ethical standards of the institution and with the Declaration of Helsinki.

Sample Preparation, Library Generation, and Sequencing

scDNA-seq. Single-cell library DNA prep was performed using the Tapestri platform and reagents (MissionBio) according to the manufacturer's instructions. Briefly, cryopreserved cells were thawed, washed with PBS, and manually counted using a hemocytometer. Cells were normalized to 5,000 cells/μL using a Cell Buffer (MissionBio). Next, samples were loaded into a microfluidics cartridge where individual cells in conjunction with lysis buffer were encapsulated into water-in-oil droplets using the Tapestri instrument. Encapsulated cells were tagged with a unique barcode, and the DNA from barcoded cells was amplified via multiplex PCR using a targeted myeloid panel that included 312 amplicons across 47 genes known to be associated with myeloid malignancies (Supplementary Tables S9 and S10). Next, amplified cellular DNA was released from individual oil droplets and purified using Ampure XP beads (Beckman Coulter). Libraries were generated by incorporating dual i5/i7 indices and library template (MissionBio) with the purified PCR products during a second PCR and purified again with Ampure XP beads. The final product was quantified via Qubit fluorometer (Thermo Fisher) and assessed for quality using an Agilent Bioanalyzer. Samples were pooled prior to sequencing with a 25% spike-in of PhiX and run on a NovaSeq 6000 (Illumina) S4 flow cell to generate 150 bp paired-end reads. Sequencing was performed at the Vanderbilt Technologies for Advanced Genomics (VANTAGE) sequencing core.

scDNA-seq with Antibody–Oligonucleotide Conjugates. Samples for combined AOC-based protein detection were prepared in the same manner as described above with the following modifications. Cells were normalized to 10,000 cells/μL in 100 μL and incubated with 10 mg/mL dextran sulfate (Research Products International), Human TruStain FcX (BioLegend), and 1× staining buffer (MissionBio) for 3 minutes at ambient temperature. Next, cells were stained with a combination of 13 AOCs (Supplementary Table S8; MissionBio) for 30 minutes at ambient temperature. Following staining, cells were washed three times in Dulbecco's PBS (Gibco), recounted, and processed as above with the addition of adding 2 μmol/L antibody tag forward primer (Tapestri) prior to the barcoding step. DNA libraries were prepared and purified as above. Protein PCR products, which exist in the supernatant from the Ampure XP bead purification step, were isolated by a 5-minute incubation with 2 μL 5′ Biotin Oligo (IDT) for 5 minutes at 96°C, followed by a 5-minute incubation on ice. Isolated proteins were washed using 2× binding and washing buffer (10 mmol/L Tris-HCL, 1 mmol/L EDTA, 2 M NaCl) and streptavidin beads (Thermo Fisher). Protein libraries were generated using the washed proteins, library template (MissionBio), and i5/i7 indices (IDT) via PCR. The protein library PCR product was cleaned again using Ampure XP beads. Both DNA and protein libraries were quantified, quality checked, and sequenced as above.

scRNA-seq. scRNA-seq libraries were created from viable patient-derived samples using the 10X Chromium 5′ library (patient 17) or 10X Chromium 3′ v1 (patient 3) preparation kits (10X Genomics) using the manufacturer's recommendations and targeting 10,000 cells per sample. Next-generation 150 nt paired-end sequencing was performed on an Illumina Novaseq6000. Low quality reads were filtered out and CellRanger Count v3.1 (patient 17) or v6.1 (patient 3) (10X Genomics) was used to align reads onto the GRCh38 reference genome. Downstream analysis was performed as below.

Bulk DNA-seq. Bulk sequencing from clinical sample sequencing was used when available to corroborate variants. When available, clinical bulk-sequencing results were used. In instances where this testing was not performed and remaining patient cells existed, Archer Dx kits were used to perform bulk-sequencing sample prep and library generation as described previously (Supplementary Table S11; ref. 58).

Data Analysis

Pipeline Processing and Variant Filtering. FASTQ files from single-cell DNA samples were processed via the Tapestri Pipeline v1.8.4. Adapters were trimmed using Cutadapt (59, 60), and reads longer than 30 nt were aligned to the hg19 reference genome with BWA-MEM (61). Cells were then called based on amplicon-read completeness in each barcode. Variants were called using GATK 3.7

(62) with a joint-calling approach that follows GATK best practices (63, 64). Then, the variant lists were decomposed, filtered, and the genotype/cell matrix loaded into the Tapestri Insights software package (v.2.2) where low-quality cells and variants were removed based on genotype quality score <30, variants genotyped in <50% of cells, read depth <10 reads, cells with <50% of genotypes present, cells with genotypes of <20% alternate allele frequencies, and variants mutated in <0.5% of cells. For some pathogenic mutations that were poorly genotyped, e.g., *IDH2*R172 and *SRSF2*P95, we had to lower the "exclude variants genotyped in <50% of cells" parameter to exclude variants genotyped in <20% of cells. Using five apparent heterozygous germline variants in each sample, the allele dropout (ADO) was calculated using the following formula for each of the five variants: [(# of wild-type cells + # of homozygous cells)/total number of cells genotyped] × 100 (Supplementary Table S3). The data were further analyzed in R, including the Tapestri package.

Mutational and Clonal Analysis. Variants filtered as above were then assessed for known pathogenicity or likely pathogenicity via ClinVar and Varsome databases (65, 66). Nonintronic, previously identified somatic variants were included in clonal analyses. The clonal architecture of each sample was determined using genotype clustering and zygosity information in Tapestri Insights (Mission Bio). Serial samples from an individual patient (MDS and sAML samples) were analyzed concurrently and compared to determine clonal progression. Clones with <10 cells were excluded unless the same clone was also observed at another time point in the same patient. Oncoprints were constructed from sample-level and cell-level variant information using the R ComplexHeatmap package (67). Set interaction analysis was visualized with the UpSetR package (68). Clonal prevalence plots of the temporal clonal evolution data were generated from clonal phylogeny and clonal prevalence at MDS and sAML time points using the Timescape package (69).

Single-Cell Protein Analysis. FASTQ files from single-cell protein samples were processed by Mission Bio. The input FASTQ files were first validated to identify the run chemistry and check the sequence quality using the fastp tool (70). Adapters were trimmed and short reads were removed. Next, PCR handle and capture sequences were trimmed, and the antibody barcodes were extracted from R2 reads and corrected using the error correction map. Output count files were then generated. For the three patients for whom we also had antibody barcoding data (patients 14, 17, and 18), we explored the intersect of genotype call and protein marker identity, following centered log-ratio transformation of the multiomics data derived from the same barcodes.

scRNA-seq Analysis. scRNA-seq data were obtained from a 10X Genomics Chromium-based CITE-Seq experiment. After processing via Cell Ranger, two samples from patient 17 yielded a combined 9,606 cells and 33,538 genes. The data were filtered in Seurat to include at least 500 RNA molecules per cell, at least 250 genes per cell, at least 0.8 of the $\log_{10}$ value of genes per UMI ($\log_{10}$GenesPerUMI), and a proportion of transcripts mapping to mitochondrial genes less than 15%. Only genes that had a nonzero expression value in at least 10 cells were preserved, resulting in a final data set of 6,863 cells and 15,359 genes. Samples from patient 3 were demultiplexed and filtered using the same parameters as the patient 17 analysis, resulting in a final data set of 7,100 cells and 18,099 genes.

The sample-level data were normalized using the SCTransform method (71), which utilizes a regularized negative binomial regression for normalization and variance stabilization. Furthermore, it estimates the variance of the raw filtered data, identifies the most variable genes, and regresses out mitochondrial mapping contribution as a confounding source of variation. After review, the UMAP embeddings of the normalized data revealed a misalignment of the two samples. We, therefore, integrated the data sets using Seurat's canonical correlation analysis method (72), using the top 5,000 features as the integration selection. Standard exploratory data analysis methods were used to identify cell populations and quantify gene-expression differences between these populations.

Pseudo-Bulk Differential Gene-Expression Analysis. To mitigate the effects of false discoveries and bias toward highly expressed genes in single-cell DE analysis methods, we opted for a pseudo-bulk method (73). For patients 3 and 17 single-cell data, cells associated with primitive and mature myeloid clusters were split by condition (MDS and sAML) resulting in patient-specific single-cell data sets: primitive-MDS, primitive-sAML, mature-MDS, and mature-sAML. For each data set, we generated pseudo-samples by applying a binomial distribution to randomly distribute single cells into sample groups. Then, for each sample group, the raw counts per gene were summed to generate an ensemble of pseudo-bulk input files. Per patient, we applied DESeq2, to independently study the differential gene expression of sAML versus MDS, for primitive and mature cell populations (74).

GSEA. GSEA was performed using Fast GSEA using preranked lists and Molecular Signatures Database v7.1 Hallmark gene sets, which represent well-defined biological states or processes (75, 76). The preranked lists were generated from the fold change and adjusted *P*-value results of the DESeq2-derived differentially expressed genes between sAML and MDS, on a per patient and metacluster basis.

Statistical Analysis

Statistical significance was set at $P < 0.05$. For pairwise comparisons, we used a two-sided Student *t* test or Wilcoxon rank-sum test as indicated. For comparison of multiple groups, we used a one-way analysis of variance test in R. To evaluate nonrandom associations of mutational identities in the three pattern groups, we used a Fisher exact test. Kaplan–Meier plots and Cox proportional hazard modeling were done in R using packages *survival* (https://github.com/therneau/survival) and *survminer* (https://github.com/kassambara/survminer). The Shannon diversity index was calculated as described previously using clone identity and number for each sample in place of species (77). Plots were created using the packages *dplyr*, *tidyr*, *ggpubr*, and *ggplot2* in R (version 4.1.0) within RStudio (version 1.4.1717; ref. 78).

Data Availability Statement

Deidentified single-cell and bulk DNA sequencing data have been deposited at NCBI Sequence Read Archive in BioProject PRJNA831862. Single-cell RNA-seq data are available in the Gene Expression Omnibus (GEO) repository under accession number GSE205490.

Authors' Disclosures

M.R. Savona reports personal fees from AbbVie, BMS, CTI, Sierra Oncology, Novartis, grants from Astex and Incyte, personal fees and other support from Karyopharm, Ryvu, personal fees from Sierra Oncology, grants and personal fees from Takeda, and TG Therapeutics outside the submitted work. P.B. Ferrell reports grants from Incyte, Astex Pharmaceuticals, and Forma Therapeutics outside the submitted work. No disclosures were reported by the other authors.

Authors' Contributions

T. Guess: Conceptualization, data curation, formal analysis, supervision, validation, investigation, visualization, methodology, writing–original draft, project administration, writing–review and editing. **C.R. Potts:** Formal analysis, validation, investigation, methodology, writing–review and editing. **P. Bhat:** Data curation, software, formal analysis, validation, investigation, visualization, methodology, writing–review and editing. **J.A. Cartailler:** Data curation, software, formal analysis, validation, investigation, visualization, methodology, writing–review and editing. **A. Brooks:** Formal analysis, investigation. **C. Holt:** Software, formal analysis, investigation, visualization, writing–review and editing. **A. Yenamandra:** Data curation, writing–review and editing. **F.C. Wheeler:** Data curation, writing–review and

editing. **M.R. Savona:** Resources, project administration, writing–review and editing. **J.-P. Cartailler:** Conceptualization, data curation, software, formal analysis, validation, investigation, visualization, methodology, writing–original draft, writing–review and editing. **P.B. Ferrell:** Conceptualization, resources, data curation, software, formal analysis, supervision, funding acquisition, validation, investigation, visualization, methodology, writing–original draft, project administration, writing–review and editing.

Acknowledgments

Patient samples were supplied by the Vanderbilt Hematologic Malignancy Tissue Repository, a Vanderbilt-Ingram Cancer Center (VICC)- and VUMC-supported resource. We acknowledge Vanderbilt Technologies for Advanced Genomics (VANTAGE) for help with sequencing. We thank Angela Jones at VANTAGE for her sequencing expertise and advice throughout the project. We gratefully acknowledge Robert Durruthy-Durruthy, Jose Jacob, Yue Wang, Kelly Kaihara, and all other members of MissionBio for the technical support, analytical help, and genomics expertise. We also thank Crystal Amsberry from ArcherDx for her assistance with sequencing and analysis. This work was supported by a VICC Ambassadors Award (P.B. Ferrell), a Vanderbilt Institute for Clinical and Translation Research Clinical Translational Science Award Program 5UL1TR002243 (P.B. Ferrell and T. Guess), NIH K23HL138291 (P.B. Ferrell). M.R. Savona is supported by NIH 1R01CA262287 and 1U01OH012271, an LLS Clinical Scholar Award, the Biff Ruttenburg Foundation, the Adventure Alle Fund, the Beverly and George Rawlings Research Directorship, the E.P. Evans MDS Foundation.

Note

Supplementary data for this article are available at Blood Cancer Discovery Online (https://bloodcancerdiscov.aacrjournals.org/).

Received August 17, 2021; revised February 22, 2022; accepted May 4, 2022; published first May 6, 2022.

REFERENCES

1. Kuykendall A, Duployez N, Boissel N, Lancet JE, Welch JS. Acute myeloid leukemia: the good, the bad, and the ugly. Am Soc Clin Oncol Educ Book 2018;38:555–73.
2. Bennett JM. Secondary acute myeloid leukemia. Leuk Res 1995;19:231–2.
3. Weinberg OK, Seetharam M, Ren L, Seo K, Ma L, Merker JD, et al. Clinical characterization of acute myeloid leukemia with myelodysplasia-related changes as defined by the 2008 WHO classification system. Blood 2009;113:1906–8.
4. Nowell PC. The clonal evolution of tumor cell populations. Science 1976;194:23–8.
5. Greaves M, Maley CC. Clonal evolution in cancer. Nature 2012;481:306–13.
6. Shlush LI, Mitchell A, Heisler L, Abelson S, Ng SWK, Trotman-Grant A, et al. Tracing the origins of relapse in acute myeloid leukaemia to stem cells. Nature 2017;547:104–8.
7. Kroeger H, Jelinek J, Estécio MRH, He R, Kondo K, Chung W, et al. Aberrant CpG island methylation in acute myeloid leukemia is accentuated at relapse. Blood 2008;112:1366–73.
8. Ding L, Ley TJ, Larson DE, Miller CA, Koboldt DC, Welch JS, et al. Clonal evolution in relapsed acute myeloid leukaemia revealed by whole-genome sequencing. Nature 2012;481:506–10.
9. Klco JM, Spencer DH, Miller CA, Griffith M, Lamprecht TL, O'Laughlin M, et al. Functional heterogeneity of genetically defined subclones in acute myeloid leukemia. Cancer Cell 2014;25:379–92.
10. Walter MJ, Shen D, Ding L, Shao J, Koboldt DC, Chen K, et al. Clonal architecture of secondary acute myeloid leukemia. N Engl J Med 2012;366:1090–8.
11. Walter MJ, Shen D, Shao J, Ding L, White BS, Kandoth C, et al. Clonal diversity of recurrently mutated genes in myelodysplastic syndromes. Leukemia 2013;27:1275–82.
12. Makishima H, Yoshizato T, Yoshida K, Sekeres MA, Radivoyevitch T, Suzuki H, et al. Dynamics of clonal evolution in myelodysplastic syndromes. Nat Genet 2017;49:204–12.
13. Chen J, Kao YR, Sun D, Todorova TI, Reynolds D, Narayanagari SR, et al. Myelodysplastic syndrome progression to acute myeloid leukemia at the stem cell level. Nat Med 2019;25:103–10.
14. Menssen AJ, Walter MJ. Genetics of progression from MDS to secondary leukemia. Blood 2020;136:50–60.
15. Miles LA, Bowman RL, Merlinsky TR, Csete IS, Ooi AT, Durruthy-Durruthy R, et al. Single-cell mutation analysis of clonal evolution in myeloid malignancies. Nature 2020;587:477–82.
16. Morita K, Wang F, Jahn K, Hu T, Tanaka T, Sasaki Y, et al. Clonal evolution of acute myeloid leukemia revealed by high-throughput single-cell genomics. Nat Commun 2020;11:5327.
17. Pellegrino M, Sciambi A, Treusch S, Durruthy-Durruthy R, Gokhale K, Jacob J, et al. High-throughput single-cell DNA sequencing of acute myeloid leukemia tumors with droplet microfluidics. Genome Res 2018;28:1345–52.
18. Ediriwickrema A, Aleshin A, Reiter JG, Corces MR, Kohnke T, Stafford M, et al. Single-cell mutational profiling enhances the clinical evaluation of AML MRD. Blood Adv 2020;4:943–52.
19. Taylor J, Mi X, North K, Binder M, Penson A, Lasho T, et al. Single-cell genomics reveals the genetic and molecular bases for escape from mutational epistasis in myeloid neoplasms. Blood 2020;136:1477–86.
20. Kennedy AL, Myers KC, Bowman J, Gibson CJ, Camarda ND, Furutani E, et al. Distinct genetic pathways define pre-leukemic and compensatory clonal hematopoiesis in Shwachman-Diamond syndrome. bioRxiv 2020:2020.06.04.134692.
21. Alberti-Servera L, Demeyer S, Govaerts I, Swings T, De Bie J, Gielen O, et al. Single-cell DNA amplicon sequencing reveals clonal heterogeneity and evolution in T-cell acute lymphoblastic leukemia. Blood 2021;137:801–11.
22. Dillon LW, Ghannam J, Nosiri C, Gui G, Goswami M, Calvo KR, et al. Personalized single-cell proteogenomics to distinguish acute myeloid leukemia from non-malignant clonal hematopoiesis. Blood Cancer Discov 2021;2:319–25.
23. Benard BA, Leak LB, Azizi A, Thomas D, Gentles AJ, Majeti R. Clonal architecture predicts clinical outcomes and drug sensitivity in acute myeloid leukemia. Nat Commun 2021;12:7244.
24. Eastburn DJ, Huang Y, Pellegrino M, Sciambi A, Ptacek LJ, Abate AR. Microfluidic droplet enrichment for targeted sequencing. Nucleic Acids Res 2015;43:e86.
25. Xu L, Durruthy-Durruthy R, Eastburn DJ, Pellegrino M, Shah O, Meyer E, et al. Clonal evolution and changes in two AML patients detected with a novel single-cell DNA sequencing platform. Sci Rep 2019;9:11119.
26. Lindsley RC, Mar BG, Mazzola E, Grauman PV, Shareef S, Allen SL, et al. Acute myeloid leukemia ontogeny is defined by distinct somatic mutations. Blood 2015;125:1367–76.
27. Ogawa S. Genetics of MDS. Blood 2019;133:1049–59.
28. Papaemmanuil E, Gerstung M, Bullinger L, Gaidzik VI, Paschka P, Roberts ND, et al. Genomic classification and prognosis in acute myeloid leukemia. N Engl J Med 2016;374:2209–21.
29. Grove CS, Vassiliou GS. Acute myeloid leukaemia: a paradigm for the clonal evolution of cancer? Dis Model Mech 2014;7:941–51.
30. McMahon CM, Ferng T, Canaani J, Wang ES, Morrissette JJD, Eastburn DJ, et al. Clonal selection with RAS pathway activation mediates secondary clinical resistance to selective FLT3 inhibition in acute myeloid leukemia. Cancer Discov 2019;9:1050–63.
31. Menssen AJ, Khanna A, Miller CA, Srivatsan SN, Chang GS, Shao J, et al. Convergent clonal evolution of signaling gene mutations is a hallmark of myelodysplastic syndrome progression. Blood Cancer Discov 2022;3:330–45.
32. Cerami E, Gao J, Dogrusoz U, Gross BE, Sumer SO, Aksoy BA, et al. The cBio cancer genomics portal: an open platform for exploring multidimensional cancer genomics data. Cancer Discov 2012;2:401–4.
33. Gao J, Aksoy BA, Dogrusoz U, Dresdner G, Gross B, Sumer SO, et al. Integrative analysis of complex cancer genomics and clinical profiles using the cBioPortal. Sci Signal 2013;6:pl1.

34. Haase D, Stevenson KE, Neuberg D, Maciejewski JP, Nazha A, Sekeres MA, et al. TP53 mutation status divides myelodysplastic syndromes with complex karyotypes into distinct prognostic subgroups. Leukemia 2019;33:1747–58.
35. Bernard E, Nannya Y, Hasserjian RP, Devlin SM, Tuechler H, Medina-Martinez JS, et al. Implications of TP53 allelic state for genome stability, clinical presentation and outcomes in myelodysplastic syndromes. Nat Med 2020;26:1549–56.
36. DiNardo CD, Cortes JE. Mutations in AML: prognostic and therapeutic implications. Hematology Am Soc Hematol Educ Program 2016;2016:348–55.
37. Man CH, Fung TK, Ho C, Han HH, Chow HC, Ma AC, et al. Sorafenib treatment of FLT3-ITD(+) acute myeloid leukemia: favorable initial outcome and mechanisms of subsequent nonresponsiveness associated with the emergence of a D835 mutation. Blood 2012;119:5133–43.
38. Demaree B, Delley CL, Vasudevan HN, Peretz CAC, Ruff D, Smith CC, et al. Joint profiling of DNA and proteins in single cells to dissect genotype-phenotype associations in leukemia. Nat Commun 2021;12:1583.
39. Campello RJGB, Moulavi D, Sander J. Density-based clustering based on hierarchical density estimates. Advances in knowledge discovery and data mining. Berlin, Heidelberg: Springer Berlin Heidelberg; 2013. p. 160–72.
40. McInnes L, Healy J. Accelerated hierarchical density based clustering. 2017 IEEE International Conference on Data Mining Workshops (ICDMW) 2017:33–42.
41. Deng M, Gui X, Kim J, Xie L, Chen W, Li Z, et al. LILRB4 signalling in leukaemia cells mediates T cell suppression and tumour infiltration. Nature 2018;562:605–9.
42. Humbert M, Halter V, Shan D, Laedrach J, Leibundgut EO, Baerlocher GM, et al. Deregulated expression of Kruppel-like factors in acute myeloid leukemia. Leuk Res 2011;35:909–13.
43. Chung SS, Eng WS, Hu W, Khalaj M, Garrett-Bakelman FE, Tavakkoli M, et al. CD99 is a therapeutic target on disease stem cells in myeloid malignancies. Sci Transl Med 2017;9:eaaj2025.
44. Blatt K, Herrmann H, Hoermann G, Willmann M, Cerny-Reiterer S, Sadovnik I, et al. Identification of campath-1 (CD52) as novel drug target in neoplastic stem cells in 5q-patients with MDS and AML. Clin Cancer Res 2014;20:3589–602.
45. Eisenwort G, Sadovnik I, Keller A, Ivanov D, Peter B, Berger D, et al. Phenotypic characterization of leukemia-initiating stem cells in chronic myelomonocytic leukemia. Leukemia 2021;35:3176–87.
46. Jin L, Hope KJ, Zhai Q, Smadja-Joffe F, Dick JE. Targeting of CD44 eradicates human acute myeloid leukemic stem cells. Nat Med 2006;12:1167–74.
47. Scholl C, Frohling S, Dunn IF, Schinzel AC, Barbie DA, Kim SY, et al. Synthetic lethal interaction between oncogenic KRAS dependency and STK33 suppression in human cancer cells. Cell 2009;137:821–34.
48. Izzo F, Lee SC, Poran A, Chaligne R, Gaiti F, Gross B, et al. DNA methylation disruption reshapes the hematopoietic differentiation landscape. Nat Genet 2020;52:378–87.
49. Zhang X, Su J, Jeong M, Ko M, Huang Y, Park HJ, et al. DNMT3A and TET2 compete and cooperate to repress lineage-specific transcription factors in hematopoietic stem cells. Nat Genet 2016;48:1014–23.
50. Challen GA, Sun D, Jeong M, Luo M, Jelinek J, Berg JS, et al. Dnmt3a is essential for hematopoietic stem cell differentiation. Nat Genet 2011;44:23–31.
51. Yoshizato T, Dumitriu B, Hosokawa K, Makishima H, Yoshida K, Townsley D, et al. Somatic mutations and clonal hematopoiesis in aplastic anemia. N Engl J Med 2015;373:35–47.
52. Lundgren S, Keranen MAI, Kankainen M, Huuhtanen J, Walldin G, Kerr CM, et al. Somatic mutations in lymphocytes in patients with immune-mediated aplastic anemia. Leukemia 2021;35:1365–79.
53. Vercauteren SM, Starczynowski DT, Sung S, McNeil K, Salski C, Jensen CL, et al. T cells of patients with myelodysplastic syndrome are frequently derived from the malignant clone. Br J Haematol 2012;156:409–12.
54. Petti AA, Williams SR, Miller CA, Fiddes IT, Srivatsan SN, Chen DY, et al. A general approach for detecting expressed mutations in AML cells using single cell RNA-sequencing. Nat Commun 2019;10:3660.
55. Christopher MJ, Petti AA, Rettig MP, Miller CA, Chendamarai E, Duncavage EJ, et al. Immune escape of relapsed AML cells after allogeneic transplantation. N Engl J Med 2018;379:2330–41.
56. Corey SJ, Minden MD, Barber DL, Kantarjian H, Wang JC, Schimmer AD. Myelodysplastic syndromes: the complexity of stem-cell diseases. Nat Rev Cancer 2007;7:118–29.
57. Vardiman JW, Thiele J, Arber DA, Brunning RD, Borowitz MJ, Porwit A, et al. The 2008 revision of the World Health Organization (WHO) classification of myeloid neoplasms and acute leukemia: rationale and important changes. Blood 2009;114:937–51.
58. Crowgey EL, Mahajan N, Wong WH, Gopalakrishnapillai A, Barwe SP, Kolb EA, et al. Error-corrected sequencing strategies enable comprehensive detection of leukemic mutations relevant for diagnosis and minimal residual disease monitoring. BMC Med Genomics 2020;13:32.
59. Martin M. Cutadapt removes adapter sequences from high-throughput sequencing reads. EMBnetjournal 2011;17:10–2.
60. Bolger AM, Lohse M, Usadel B. Trimmomatic: a flexible trimmer for Illumina sequence data. Bioinformatics 2014;30:2114–20.
61. Li H, Durbin R. Fast and accurate long-read alignment with Burrows-Wheeler transform. Bioinformatics 2010;26:589–95.
62. McKenna A, Hanna M, Banks E, Sivachenko A, Cibulskis K, Kernytsky A, et al. The Genome Analysis Toolkit: a MapReduce framework for analyzing next-generation DNA sequencing data. Genome Res 2010;20:1297–303.
63. Van der Auwera GA, Carneiro MO, Hartl C, Poplin R, Del Angel G, Levy-Moonshine A, et al. From FastQ data to high confidence variant calls: the Genome Analysis Toolkit best practices pipeline. Curr Protoc Bioinformatics 2013;43:11 0 1–0 33.
64. DePristo MA, Banks E, Poplin R, Garimella KV, Maguire JR, Hartl C, et al. A framework for variation discovery and genotyping using next-generation DNA sequencing data. Nat Genet 2011;43:491–8.
65. Kopanos C, Tsiolkas V, Kouris A, Chapple CE, Albarca Aguilera M, Meyer R, et al. VarSome: the human genomic variant search engine. Bioinformatics 2018;35:1978–80.
66. Landrum MJ, Lee JM, Benson M, Brown GR, Chao C, Chitipiralla S, et al. ClinVar: improving access to variant interpretations and supporting evidence. Nucleic Acids Res 2018;46:D1062–D7.
67. Gu Z, Eils R, Schlesner M. Complex heatmaps reveal patterns and correlations in multidimensional genomic data. Bioinformatics 2016;32:2847–9.
68. Conway JR, Lex A, Gehlenborg N. UpSetR: an R package for the visualization of intersecting sets and their properties. Bioinformatics 2017;33:2938–40.
69. Smith MA, Nielsen CB, Chan FC, McPherson A, Roth A, Farahani H, et al. E-scape: interactive visualization of single-cell phylogenetics and cancer evolution. Nat Methods 2017;14:549–50.
70. Chen S, Zhou Y, Chen Y, Gu J. fastp: an ultra-fast all-in-one FASTQ preprocessor. Bioinformatics 2018;34:i884–i90.
71. Hafemeister C, Satija R. Normalization and variance stabilization of single-cell RNA-seq data using regularized negative binomial regression. Genome Biol 2019;20:296.
72. Stuart T, Butler A, Hoffman P, Hafemeister C, Papalexi E, Mauck WM 3rd, et al. Comprehensive integration of single-cell data. Cell 2019;177:1888–902.
73. Squair JW, Gautier M, Kathe C, Anderson MA, James ND, Hutson TH, et al. Confronting false discoveries in single-cell differential expression. Nat Commun 2021;12:5692.
74. Love MI, Huber W, Anders S. Moderated estimation of fold change and dispersion for RNA-seq data with DESeq2. Genome Biol 2014;15:550.
75. Liberzon A, Birger C, Thorvaldsdottir H, Ghandi M, Mesirov JP, Tamayo P. The Molecular Signatures Database (MSigDB) hallmark gene set collection. Cell Syst 2015;1:417–25.
76. Korotkevich G, Sukhov V, Budin N, Shpak B, Artyomov MN, Sergushichev A. Fast gene set enrichment analysis. bioRxiv 2021:060012.
77. Spellerberg IF, Fedor PJ. A tribute to Claude Shannon (1916–2001) and a plea for more rigorous use of species richness, species diversity and the 'Shannon–Wiener' Index. Global Ecol Biogeogr 2003;12:177–9.
78. Wickham H. ggplot2: elegant graphics for data analysis. New York: Springer-Verlag; 2016.